# Tunable electronic structure in gallium chalcogenide van der Waals compounds

Brian Shevitski , 1,2,\* Søren Ulstrup, 3,4,\*,† Roland J. Koch, Hui Cai, Sefaattin Tongay, Luca Moreschini, Chris Jozwiak, Aaron Bostwick, Alex Zettl, Eli Rotenberg, and Shaul Aloni<sup>2,‡</sup>

<sup>1</sup>Department of Physics, University of California at Berkeley, Berkeley, California 94720,USA

<sup>&</sup>lt;sup>4</sup>Department of Physics and Astronomy, Interdisciplinary Nanoscience Center (iNANO), Aarhus University, 8000 Aarhus C, Denmark <sup>5</sup>School for Engineering of Matter, Transport and Energy, Arizona State University, Tempe, Arizona 85287, USA



(Received 2 August 2019; revised manuscript received 19 September 2019; published 9 October 2019)

Transition-metal monochalcogenides comprise a class of two-dimensional materials with electronic band gaps that are highly sensitive to material thickness and chemical composition. Here, we explore the tunability of the electronic excitation spectrum in GaSe by using angle-resolved photoemission spectroscopy. The electronic structure of the material is modified by in situ potassium deposition as well as by forming  $GaS_xSe_{1-x}$  alloy compounds. We find that potassium-dosed samples exhibit a substantial change of the dispersion around the valence-band maximum (VBM). The observed band dispersion resembles that of a single tetralayer and is consistent with a transition from the direct-gap character of the bulk to the indirect-gap character expected for monolayer GaSe. Upon alloying with sulfur, we observe a phase transition from AB to AA' stacking. Alloying also results in a rigid energy shift of the VBM towards higher binding energies, which correlates with a blueshift in the luminescence. The increase of the band gap upon sulfur alloying does not appear to change the dispersion or character of the VBM appreciably, implying that it is possible to engineer the gap of these materials while maintaining their salient electronic properties.

DOI: 10.1103/PhysRevB.100.165112

# I. INTRODUCTION

The ability to isolate monolayers and study their physical properties has led to a resurgence of interest in layered van der Waals (VDW) materials as two-dimensional systems. Transition-metal chalcogenides belong to this class of materials and demonstrate unique thermoelectric, photonic, and electronic properties [1]. The composition, phase, and crystal structure of these materials can be tuned to display a wide range of electronic phases, including metallic [2,3], semiconducting [4–6], superconducting [7–9] and charge-density wave [9-11], inspiring their use in a wide range of applications, including electronic devices, sensors, and quantum devices [12].

In their bulk form, monochalcogenides of Ga and In, such as GaSe, InSe, and GaS are van der Waals compounds. Gallium chalcogenides (GCs) are direct-band-gap semiconductors that can be mechanically exfoliated from a bulk parent crystal. Their properties are highly sensitive to material thickness, chemical composition, and crystalline structure [13–15]. Bulk GaSe and GaS have direct band gaps of 2.10 and 3.05 eV, respectively, and transition to indirect gaps when the number of layers is reduced [16,17]. Monolayer field effect devices maintain mobilities on the order of  $0.1 \text{ cm}^2 \text{ V}^{-1} \text{ s}^{-1}$ , on/off ratios of 10<sup>4</sup>-10<sup>5</sup> as well as quantum efficiencies that

exceed those of graphene by several orders of magnitude when implemented in a device architecture [18–20].

Alloys with mixed chalcogen content,  $GaS_xSe_{1-x}$ , allow for control of the band gap, allowing engineering of the optical absorption and photoluminescence (PL) [21,22]. Interlayer coupling, defects, doping, and interaction with an underlying substrate may further modify the electronic structure of GCs, as observed in exfoliated flakes of GaSe and GaTe on SiO2 and graphene [23-25] and epitaxially grown GaSe flakes on graphene [17,26,27].

In this paper, we illustrate how the crystalline and electronic properties of GC materials are affected by changes in chemical composition, doping, and reduced dimensionality using high-resolution scanning transmission electron microscopy (HRSTEM), angle-resolved photoemission spectroscopy (ARPES), and PL. HRSTEM reveals that GaSe tetralayers stack in the AB sequence ( $\varepsilon$  phase) while sulfur alloys and GaS stack almost exclusively in the AA' sequence  $(\beta \text{ phase})$ . The complete  $E(k_x, k_y, k_z)$  electronic structure of AB-stacked GaSe is determined by using ARPES, allowing us to directly extract the band dispersion along high-symmetry directions and determine valence-band (VB) extrema and effective masses. We illustrate how the full energy-momentumresolved quasiparticle band structure of the GCs is modulated when the chemical composition and/or interaction between layers is changed. We explore the influence of potassium deposition on the band structure, finding that it only causes a slight energy shift of the VBs and does not lead to degenerate doping which would enable ARPES visualization of the conduction band. However, potassium dosing does lead to a

<sup>&</sup>lt;sup>2</sup>Molecular Foundry, Lawrence Berkeley National Laboratory, Berkeley, California 94720,USA

<sup>&</sup>lt;sup>3</sup>Advanced Light Source, E. O. Lawrence Berkeley National Laboratory, Berkeley, California 94720, USA

<sup>\*</sup>These authors contributed equally to this work

<sup>†</sup>ulstrup@phys.au.dk

<sup>‡</sup>saloni@lbl.gov

significant change of the dispersion around the top of the VB, implying a strong modification at the surface GaSe tetralayer compared with the bulk. Finally, we explore the effect of sulfur alloying on the band structure. We find that increasing sulfur content produces a rigid VB shift and results in a corresponding blueshift in the PL, suggesting that alloying is a viable method for tuning GC optical properties.

#### II. EXPERIMENT

We study pure GaSe and GaS as well as three alloy compositions spanning the entire compositional range of  $GaS_xSe_{1-x}$  alloys. Crystals are grown by using the modified Bridgman-Stockbarger method [28]. Briefly, stoichiometric amounts of Ga, S, and Se powder are weighed and mixed in sealed quartz ampoules to achieve the desired alloying ratio. The ampoules are then heated in a zone furnace at 970 °C for two weeks to grow single crystals 2–8 mm in diameter.

The HRSTEM samples are prepared by a two-step process. First, the crystals are cleaved by using blue wafer dicing tape and transferred to Si substrates coated with 100-nm-thick  $SiO_2$ . Next, a Cu TEM grid with carbon film is adhered to flakes on the  $Si/SiO_2$  wafer by using a drop of isopropanol. Once the drop has dried, the  $SiO_2$  is etched away using 1 M NaOH. Lastly, the grid is washed in deionized water and dried prior to imaging. HRSTEM is carried out by using a double  $C_s$  corrected FEI Titan 80-300 operating at an accelerating voltage of 80 kV at the Molecular Foundry.

For ARPES measurements, large crystals of GCs are glued to a Cu sample holder by using epoxy and cleaved in situ in the ultrahigh-vacuum (UHV) chamber with a base pressure better than  $5 \times 10^{-11}$  mbar. The samples are cooled to 85 K prior to cleaving and kept at this temperature during ARPES measurements. The cleaved single-crystal domain sizes are on the order of 100  $\mu$ m as defined by spatially scanning the sample with the synchrotron beam. The ARPES data are collected at the Microscopic and Electronic Structure Observatory (MAE-STRO) at the Advanced Light Source (ALS) using the microARPES end-station equipped with a hemispherical Scienta R4000 analyzer. The beamline slit settings are adjusted so that the size of the beam is on the order of 20  $\mu$ m. VB and Ga 3d core-level spectra are obtained primarily by using a photon energy of 94 eV. S 2p and Se 3p core-level data are collected by using a photon energy of 300 eV. Photon energy scans of GaSe are acquired for photon energies between 21 and 140 eV. To relate the photoelectron kinetic energy Ekin to the outof-plane momentum  $k_z$ , we use the free-electron final-state assumption where  $k_z^2 = (2m/\hbar^2)(E_{kin} + V_0)$ , where  $V_0$  is the inner potential [29]. We find that  $V_0 = 10.2$  eV provides the best description of the data, given the out-of-plane lattice constant c = 15.96 Å and the Brillouin-zone (BZ) periodicity of  $2\pi/c$  for the measured polytypes of GaSe. The Fermi energy is determined on the clean Cu sample holder in contact with the crystals for all photon energies. The presence of surface photovoltage-induced energy shifts in the samples is checked by varying the photon flux. No such changes were observed, except on GaS, which excluded ARPES measurements on this material.

Potassium dosing experiments on GaSe are carried out *in situ* by using SAES getters mounted in the analysis chamber

while the sample is kept at 85 K. Each dose takes 50 seconds and, between doses, an (E,k) spectrum of the VB and an energy spectrum over the Ga 3d/K 3p binding-energy region are taken. The collection of these spectra takes 70 s and 12 doses were applied for the results presented here, amounting to a total time of 24 minutes for collecting the dataset.

Judging from the change in photoemission intensity from the VB upon further dosing, we estimate a coverage rate of a complete monolayer after 12 doses. We observe that prolonged exposure to the synchrotron beam for the fully K-dosed sample leads to broadening and significant deterioration of the quality of the spectral features, preventing detailed photon energy or angle scans for the K-dosed samples.

The total-energy and momentum resolution in the ARPES data are better than 20 meV and 0.01  $\text{Å}^{-1}$ , respectively.

#### III. RESULTS AND DISCUSSION

### A. High-resolution scanning transmission electron microscopy measurements of gallium chalcogenides

The  $GaS_xSe_{1-x}$  system forms a continuous set of alloys for the entire compositional range  $(0 \le x \le 1)$  of the stoichiometry [30–32]. Like other layered VdW materials, the intralayer bonding is strong and mostly covalent while the interlayer bonding is weak and of VdW character. The unit cell consists of two tetrahedral pyramids stacked tip to tip with chalcogen atoms at the base and a Ga atom at the apex, forming a four-atom-thick tetralayer.

The layer stacking exhibits several different polytypes, depending on composition and growth conditions. In the  $\varepsilon$  phase [Figs. 1(a) and 1(b)], successive tetralayers are stacked in the sequence AB, resulting in Ga atoms from the A layer being vertically aligned with chalcogen atoms in the B layer, and chalcogen atoms in the A layer being vertically aligned with the interstitial voids in the centers of the hexagons from the B layer, similar to Bernal stacking in graphite. The inversion-symmetric  $\beta$  phase [Figs. 1(e) and 1(f)] is obtained by stacking successive tetralayers in the sequence AA', resulting in Ga (chalcogen) atoms from the A layer eclipsing chalcogen (Ga) atoms from the A' layer. The system can also form the rhombohedral  $\gamma$  phase (ABC stacking), but this stacking sequence is not observed experimentally in our samples.

Previous studies have explored the relationship between sulfur content and stacking phase [30–32].  $GaS_xSe_{1-x}$  alloys with low sulfur content (x < 0.15) stack in the  $\varepsilon$  phase while alloys with higher sulfur content (x > 0.35) display the  $\beta$  stacking phase. Our experimental results (described below) also show this trend. We find that the  $\varepsilon$  phase occurs for  $x \le 0.3$  and the  $\beta$  phase for x > 0.3. The  $\beta$  and  $\varepsilon$  phases are thought to coexist for intermediate sulfur content (0.15 < x < 0.35) and phase segregated throughout the crystal, but our samples do not show experimental evidence for this theory.

Contrast in HRSTEM indicates differences in atomic number, density, and thickness throughout a specimen. Due to the specific stacking sequences exhibited by the polytypes of  $GaS_xSe_{1-x}$  alloys and the contrast mechanisms of STEM imaging, our imaging experiments [Figs. 1(c) and 1(g)] unambiguously reveal the stacking phases of these materials.

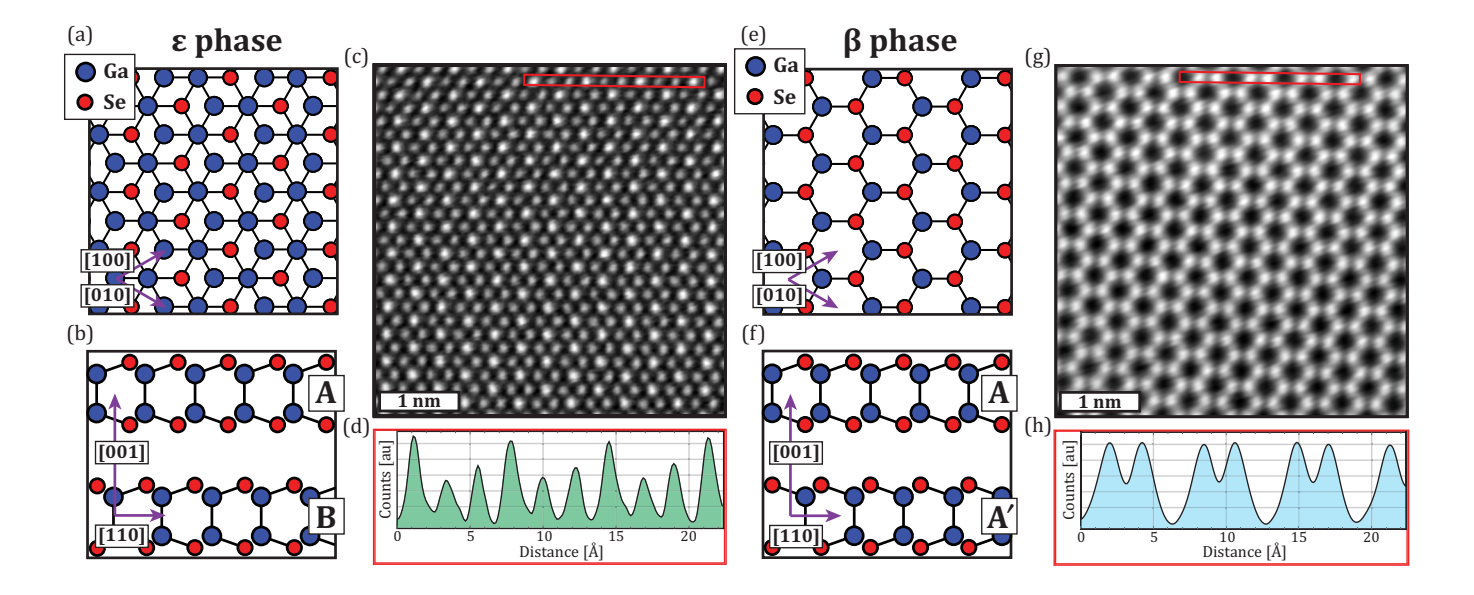


FIG. 1. Real-space structure and HRSTEM images of the two most common  $GaS_xSe_{1-x}$  polytypes. Panels (a) and (b) show the crystal structure of the  $\varepsilon$  phase in the planes defined by the axes in the labels. The corresponding HRSTEM image in panel (c) shows a trigonal lattice, resulting from the projection of Bernal (AB) stacked honeycomb layers. The intensity cut in panel (d) was obtained from the red rectangle in panel (c) and shows bright atomic columns with approximately twice the intensity of dim atomic columns. Analogous images in panels (e) and (f) show the geometry of the  $\beta$  phase. The HRSTEM image in panel (g) shows a honeycomb mesh, with no intensity in the interstitial columns between hexagonal cells.

Figure 1(c) shows a typical HRSTEM image for an alloy with high sulfur content ( $x \sim 0.75$ ), appearing as a trigonal lattice with alternating bright and dim atomic columns. Figure 1(d) shows a line plot of the intensity extracted from the region outlined by the red rectangle in Fig. 1(c). The heights of the peaks in the line trace indicate that there are approximately twice as many atoms in bright columns compared with the dim columns, consistent with the stacking geometry of the  $\varepsilon$  phase, shown in Fig. 1(b). Figure 1(g) shows an analogous image for pure GaSe which appears as a honeycomb mesh of atomic columns with no appreciable intensity in the interstitial voids between hexagons. The line profile [Fig. 1(h)] shows that the atomic columns have uniform intensity, consistent with AA' stacking exhibited by the  $\beta$  phase.

# B. Angle-resolved photoemission spectroscopy of electronic structure of GaSe

An overview of the electronic band structure of pristine GaSe is presented in Fig. 2. The data are acquired at a photon energy of 94 eV, which probes around the  $\Gamma$  point, as described by the BZ sketches in Fig. 2(a). Figures 2(b) and 2(c) show cuts along the  $\Gamma$ -K-M and  $\Gamma$ -M- $\Gamma$  high-symmetry directions, as signified by the dashed lines in Fig. 2(a). The evolution of the dispersion with binding energy is presented via the constant-binding-energy cuts in Figs. 2(d)–2(h), which reveal the trigonal symmetry of the dispersion as well as strong intensity variations between the bands in the BZs. The valence-band maximum (VBM) is situated at  $\Gamma$  and is characterized by a parabolic-shaped lobe. The location of the VBM at  $\Gamma$  is consistent with theoretical predictions that GaSe is a direct-gap semiconductor with the conduction-band minimum (CBM) also located at  $\Gamma$  [33]. Additional sub bands

dispersing towards M and K appear above binding energies of 1.5 eV. The material remains rather featureless away from  $\Gamma$ before the onset of this higher-binding-energy range, implying that most of the optical properties of GaSe will derive from the central parabolic lobe. The ARPES data discussed here are fully consistent with the electronic structure data presented in Ref. [34]. We investigate the  $k_z$  dispersion in the threedimensional BZ of GaSe shown in Fig. 3(a). By measuring the photon energy dependence of the dispersion at normal emission we are able to trace the band structure along the  $\Gamma$ -A direction, as seen in Fig. 3(b). A strong  $k_z$  dispersion is visible in the center of the parabolic lobe, which is further highlighted via the fits (open circles) and guide line in Fig. 3(b), whereas the bands at binding energies higher than 1.5 eV have a much flatter  $k_7$  dispersion. The fitted dispersion reveals an apparent BZ doubling effect; however, this occurs due to a suppression of the photoemission intensity in adjacent BZs [34], similar to observations in photoemission experiments on graphite [35,36]. The band structure along the  $\Gamma$ -K line is shown for two neighboring BZs in the  $k_z$  direction in Figs. 3(c) and 3(d). The main intensity moves from the bottom corners of the parabolic lobe in Fig. 3(c) to the VBM in Fig. 3(d). Similar intensity variations are observed in neighboring in-plane BZs, as sketched in Fig. 3(e). The  $(k_{\parallel}, k_z)$  contour at a binding energy of 0.2 eV shown in Fig. 3(f) shows a cut around the VBM for the  $\Gamma$ -A-L-M plane [see Fig. 3(e)]. The intensity maxima are seen to shift between the first and second BZs and the absolute intensity levels also vary strongly within the same BZ. A cut along the  $\Gamma$ -M line at  $k_z = 4.75 \text{ Å}^{-1}$  in Fig. 3(g) shows the upper VB parabolic lobe in two neighboring zones. In the first BZ, the intensity is concentrated in the bottom corner while in the second BZ the intensity is concentrated around the VBM. This behavior can be reconciled with the orbital character of

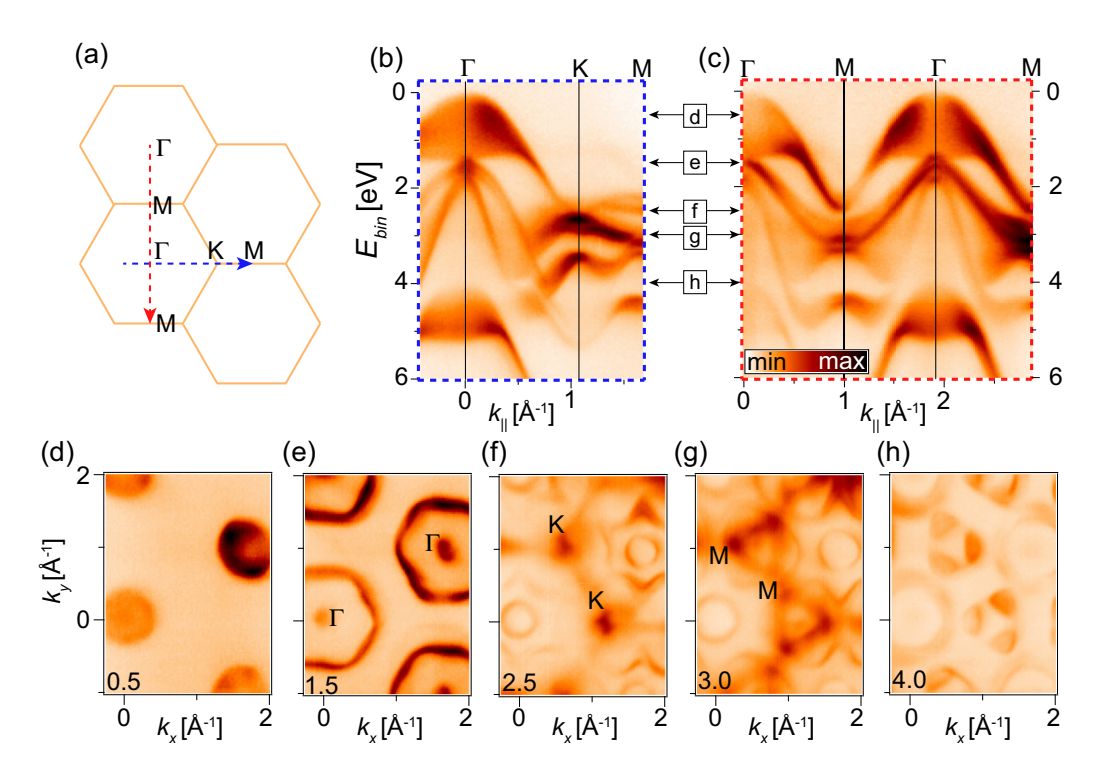


FIG. 2. ARPES measurements at a photon energy of 94 eV of the electronic structure of pristine GaSe around the  $\Gamma$  point. (a) Sketch of the BZs and their orientation in the experiment with  $\Gamma$ , K, and M symmetry points labeled. (b) Measured dispersion in the  $\Gamma$ -K-M direction obtained along the blue dashed line shown in panel (a). (c) Measured dispersion in the  $\Gamma$ -M- $\Gamma$  direction obtained along the red dashed line shown in panel (a). The double headed arrows in panels (b) and (c) indicate the planes of constant energy from which the cuts in panels (d)–(h) are taken. The energy of each cut is also listed in bottom of each panel in units of electron volts (eV). High-symmetry points  $\Gamma$ , K, and M have been labeled in panels (e)–(g), respectively.

the bands, previously studied with detailed calculations [13]. Since the states near the VBM are mainly of Se  $p_z$  character, the interlayer interactions will cause intensity modulations reflecting the coupling of the GaSe tetralayers, leading to a dispersion resembling a single tetralayer for the  $k_z$  value used for the slice shown in Fig. 3(c), while the  $k_z$  value for Fig. 3(d) shows a dispersion with a more bulk-like character [13]. The subbands just below the VBM exhibit less dramatic behavior due to the  $p_{x(y)}$  character of these states which are less sensitive to the adjacent GaSe tetralayers [37,38].

### C. Potassium deposition of GaSe

The effect of K dosing of bulk GaSe is explored in Fig. 4. Alkali-metal deposition offers the possibility to chemically donate electrons near the surface of GaSe and thereby dope the material. The ARPES measurements along the  $\Gamma$ -K-M direction in Figs. 4(a) and 4(b) before and after complete K dosing show that a significant band-structure change occurs, rather than strong electron doping. A maximum energy shift of 0.1 eV of the VB towards higher binding energies is observed, which may originate from surface band bending due to the added charge or a slight doping of the material. After further dosing, we observe that the spectral weight shifts from the top [see Fig. 4(a)] to the bottom [see Fig. 4(b)] of the VB lobe. In Fig. 4(c), the VBM dispersion (open circles), extracted via fits to energy distribution curves (EDCs), has been fit with second- and fourth-order polynomial functions in the clean and K-doped cases, respectively. In pristine GaSe,

a global VBM is observed at  $\Gamma$  and at a binding energy of  $(0.09 \pm 0.03)$  eV. The effective mass around the top of the parabola is  $m^* = (1.1 \pm 0.2)m_0$ , where  $m_0$  is the free-electron mass. In K-dosed GaSe, the VBM splits off into two maxima located at  $\pm 0.3$  Å<sup>-1</sup> with a binding energy of  $(1.30 \pm 0.04)$  eV and an effective mass of  $m^* = (1.7 \pm 0.2)m_0$ .

The EDCs extracted at normal emission in Fig. 4(d) trace the peak positions at each K-dosing step. Voigt lineshapes have been fit to each of the peaks, which have been plotted together with the photoemission intensity at normal emission at each K dose in Fig. 4(e), revealing a gradual shift of the ARPES intensity from the pristine bulk dispersion seen in Fig. 4(a) to the modified dispersion shown in Fig. 4(b). The modified dispersion strongly resembles the "bow-shape" or "inverted sombrero" dispersion of single-layer GaSe, where the inversion of the VB is characterized by the energy difference between the VBM and the local energy minimum at  $\Gamma$  [13,22,39–41]. Here, we find that the band inversion is  $(48 \pm 12)$  meV, which compares well with a value of 80 meV obtained from recent DFT calculations [40]. The value is substantially smaller than 120 meV found for singlelayer GaSe grown on graphene on silicon carbide [41] and than the value of  $(150 \pm 10)$  meV that we determine for the similar dispersion at  $k_z = 3.15 \text{ Å}^{-1}$  in Fig. 3(c). We expect that interlayer interactions between the Se  $p_z$  orbitals play a significant role for these dispersion changes around the VBM [13] and that the gradual change observed in Fig. 4(e) signals a modification of the topmost GaSe layer, leading to a weaker coupling to the underlying bulk. This may be facilitated

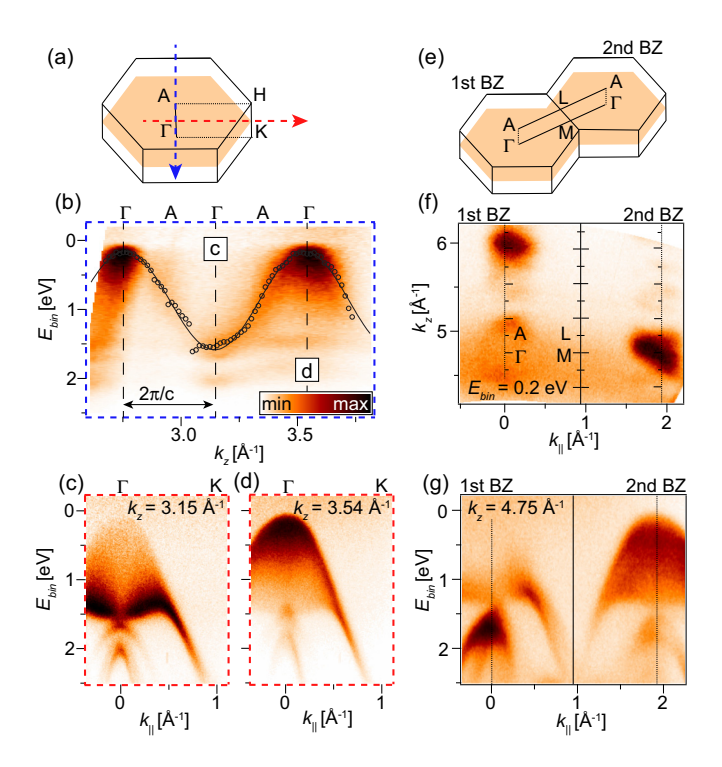


FIG. 3. ARPES measurements of the  $k_z$  dispersion of GaSe. (a) Sketch of bulk BZ highlighting the  $\Gamma$ -A-H-K plane. (b) Dispersion along the  $\Gamma$ -A direction, as marked by the blue dashed line in panel (a). Fits of the position of the VBM intensity are shown via open circles. The solid curve following the fitted dispersion is a guide for the eye. The BZ size of  $2\pi/c$  in the z direction is marked by a double-headed arrow and two vertical dashed lines. (c), (d) Dispersion extracted at the given  $k_z$  values, corresponding to the  $\Gamma$ -K direction (red dashed line). (e) Sketch of first and second BZs with an outline of the  $\Gamma$ -A-L-M plane. (f) Constant-energy contour of the plane sketched in panel (e) extracted at a binding energy of 0.2 eV with high-symmetry points annotated by tick marks. (g) Dispersion along the  $\Gamma$ -M- $\Gamma$  direction obtained at a  $k_z$  value of 4.75 Å<sup>-1</sup>.

by K intercalation in the van der Waals gap between the layers, as observed in metallic [42], and semiconducting [43] transition-metal dichalcogenides, or by a chemical interaction on the surface of the crystal, which significantly changes the coupling between individual layers, as seen in graphene multilayers [44,45]. In these situations one may also expect a change of the interlayer separation of tetralayers as well as a shift of inner potential, which also contributes to the spectral changes we observe. The possibility of chemical changes near the surface is further supported by the observation of an additional core-level component in the binding-energy range between the Ga 3d and K 3p core levels for the K-dosed sample, which is demonstrated by the comparison between the clean GaSe core-level spectrum in Fig. 4(f) and the spectrum for the fully-K-dosed sample in Fig. 4(g).

# D. Angle-resolved photoemission spectroscopy and photoluminescence measurements of $GaS_xSe_{1-x}$

 $GaS_xSe_{1-x}$  alloys offer a promising route to tune the optical gap and luminescent properties of III-VI semiconductors. However, it is unknown how robust the electronic structure

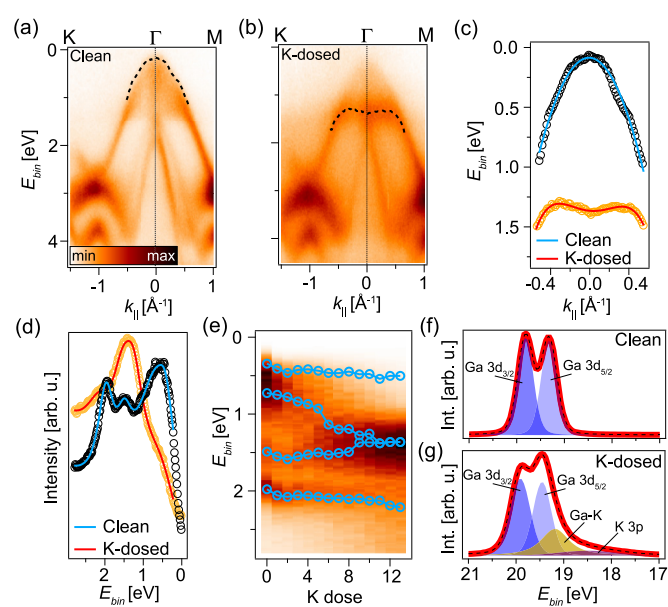


FIG. 4. Effect of K dosing on the GaSe electronic structure. (a), (b) ARPES measurements of the dispersion in the  $\Gamma$ -K-M direction (a) before and (b) after K dosing. The dashed curves present the fitted location of the VBM peak intensity. (c) Location of the VBM peak intensity (open circles) fit with a second-order and a fourthorder polynomial for the clean and K dosed samples, respectively. (d) EDCs (open circles) and results of Voigt function fits (curves) in the clean and K-dosed cases. The EDCs were extracted at  $\Gamma$  along the lines shown in panels (a) and (b). The position of the top-most peak is plotted via dashed lines in panels (a) and (b) and open circles in panels (c). (e) Evolution of the photoemission intensity at  $\Gamma$  as a function of K-dosing steps. The open circles and guidelines mark the fitted peak positions obtained by performing the EDC analysis shown in panel (d) in each K-dosing step. Ga 3d core-level measurements (f) before and (g) after K dosing. The data (thick red curves) have been fit (dashed curves) with Doniach-Sunjic lineshapes (filled peaks) for each of the observed components.

remains between different alloys. Here we compare pristine GaSe with two different  $GaS_xSe_{1-x}$  alloys (alloys I and II). The stoichiometry x is checked via core-level measurements of the Se 3p and S 2p binding-energy regions, shown in Fig. 5. By comparing the spectral weight of the Se 3p core levels, we are able to estimate that the composition of alloy I is  $x = 0.27 \pm 0.05$  and the composition of alloy II is  $x = 0.61 \pm 0.05$ 0.05. These values are consistent when we perform the same analysis on the Se 3d core levels (not shown). The core-level data are in agreement with the stoichiometry of the precursor added to the growth ampoule. Figures 6(a)-6(c) present ARPES measurements of the VBs for the three systems. The overall band dispersion is found to be very similar with a constant effective mass of  $m^* = (1.1 \pm 0.2)m_0$ . The bindingenergy position of the VBM changes significantly between the three systems, indicating a change of the electronic band gap. It is also possible that Fermi-level pinning plays a strong role for the band positions, as the defect concentration is likely different in the alloys. PL measurements, shown in Fig. 6(d), reveal a change of the optical gap. The PL peak positions plotted in Fig. 6(e) show that the optical gap increases as more S is added in the alloy. The same trend is seen for the

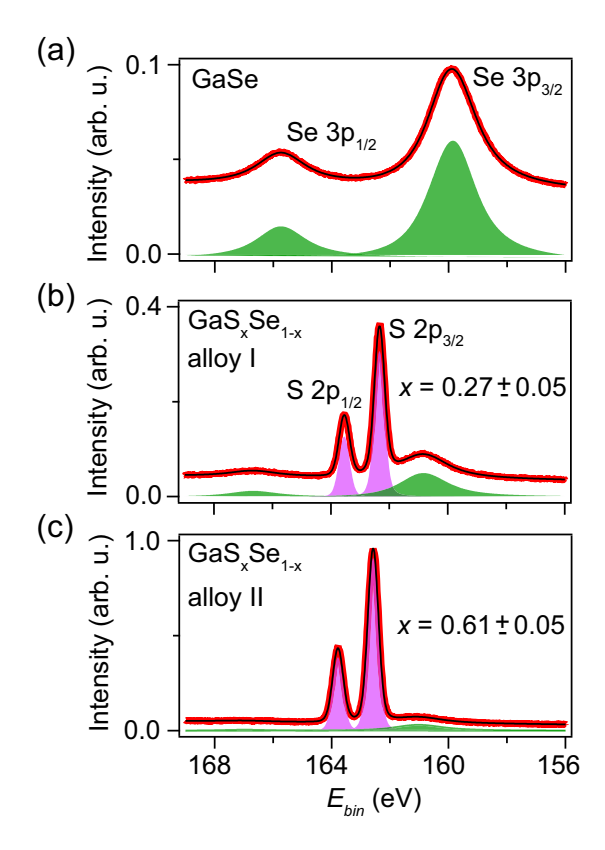


FIG. 5. Composition of  $GaS_xSe_{1-x}$  alloys from core-level data. Core-level measurements (thick red curves) in the Se 3p and S 2p binding energy region for (a) GaSe and (b), (c)  $GaS_xSe_{1-x}$  alloys. Fit results (black curves) to Doniach-Sunjic lineshapes (filled peaks) are provided in each panel. The composition x of the alloys determined via the fitted peak components is stated in panels (b) and (c). Note the intensity scale varies between the panels.

VBM binding-energy position in Fig. 6(f), which fits with a simultaneous increase of the quasiparticle band gap. The trend determined here is fully consistent with optical absorption measurements of  $GaS_xSe_{1-x}$  [22]. Note that ARPES measurements of pure GaS were attempted but the sample was found to charge too severely, which is likely due to the larger band gap of the material compared with the other  $GaS_xSe_{1-x}$  compounds investigated here.

The  $\varepsilon$  and  $\beta$  stacking phases observed in HRSTEM are not expected to give rise to striking differences in the electronic structure [37–39]. However, detailed inspection of the measurements in Fig. 6(a)–6(c) does show some variation in the intensity and structure of the dispersive bands in the higher-binding-energy region above the central VB lobe. While different stacking phases may affect the photoemission intensity, the change in chemical environment caused by the mixed chalcogen content directly influences the inplane  $p_{x(y)}$  orbitals that the higher-binding-energy bands are composed of, thereby leading to the possibility of a modified dispersion.

## IV. CONCLUSION

We have measured the bulk electronic structure of GaSe using ARPES and thereby identified the bulk band dispersion,

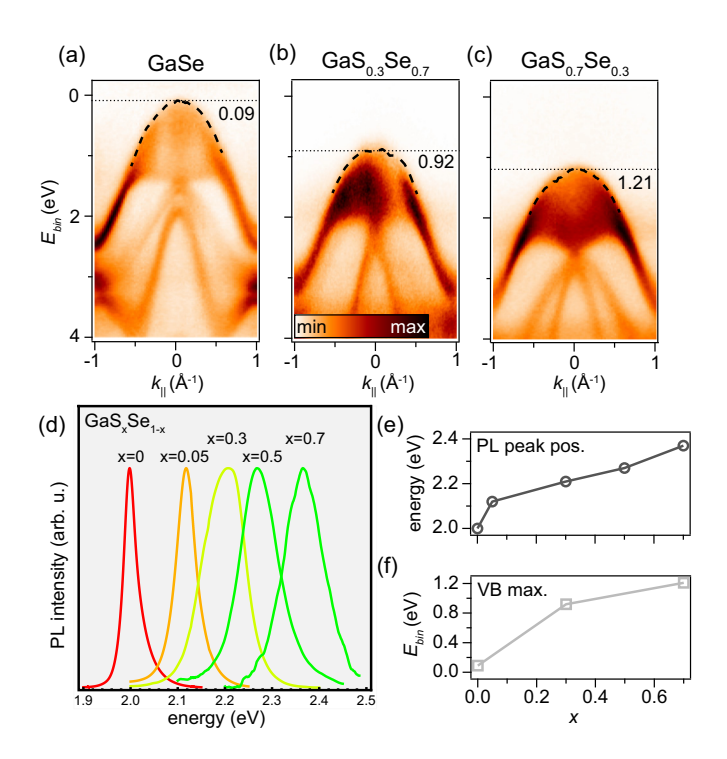


FIG. 6. VBM and PL peaks positions for  $GaS_xSe_{1-x}$  alloys. ARPES measurements of the upper VB region for (a) GaSe, (b)  $GaS_{0.27}Se_{0.73}$ , and (c)  $GaS_{0.61}Se_{0.39}$ . The dotted line presents the fitted position of the VBM and the dashed curves exhibit the fitted dispersion around the VBM in each case. The corresponding VBM binding-energy positions are given in units of eV with an error bar of  $\pm 0.03$  eV. (d) PL intensity for the same samples as in panels (a)–(c) and Fig. 5. Positions of the (e) PL peaks and (f) VBM as a function of composition.

the structure of the VBM, and the complex photoemission intensity variations associated with the tetralayer unit cell. Potassium deposition of GaSe leads to a dramatic change of the VBM dispersion from a parabolic shape characteristic for the bulk to an inverted bow-like shape that is usually associated with single-layer samples. Our data are consistent with an increased band gap and a transition from a direct to an indirect-band-gap semiconductor, which is caused by a strong modification of the top-most GaSe tetralayer due to the interaction with the deposited K atoms. We have investigated the effect of sulfur alloying on the crystalline and electronic structure and used HRSTEM to observe a transition from the  $\varepsilon$  phase to the  $\beta$  phase for sulfur content above ~30%. We have also shown that alloying causes a rigid shift of the VBM binding-energy position without a significant change in the actual band dispersion around the VBM. This rigid shift is consistent with an increase in the optical band gap measured by PL.

# ACKNOWLEDGMENTS

This work was supported primarily by the U.S. Department of Energy, Office of Science, Office of Basic Energy Sciences, Materials Sciences and Engineering Division, under Contract No. DE-AC02-05CH11231, within the van der Waals Heterostructures Program (KCWF16), which provided for

HRSTEM and ARPES support. This work was also supported in part by the National Science Foundation under Grant No. DMR-1807233, which provided for PL measurements and preliminary exploration of sample growth parameters. S.U. acknowledges financial support from VILLUM FONDEN under the Young Investigator Program (Grant No. 15375). R.J.K. was supported by a fellowship within the Postdoc-Program of the German Academic Exchange Service (DAAD). The

Advanced Light Source is supported by the Director, Office of Science, Office of Basic Energy Sciences, of the U.S. Department of Energy under Contract No. DE-AC02-05CH11231. Work at the Molecular Foundry was supported by the Office of Science, Office of Basic Energy Sciences, of the US Department of Energy under Contract No. DE-AC02-05CH11231. B.S. acknowledges support from the NSF LSAMP BD fellowship (Award No. 1249249).

- [1] M. Wasala, H. I. Sirikumara, Y. Raj Sapkota, S. Hofer, D. Mazumdar, T. Jayasekera, and S. Talapatra, Recent advances in investigations of the electronic and optoelectronic properties of group III, IV, and V selenide based binary layered compounds, J. Mater. Chem. C 5, 11214 (2017).
- [2] K. S. Novoselov, A. K. Geim, S. V. Morozov, D. Jiang, Y. Zhang, S. V. Dubonos, I. V. Grigorieva, and A. A. Firsov, Electric field effect in atomically thin carbon films, Science 306, 666 (2004).
- [3] J. Feng, X. Sun, C. Wu, L. Peng, C. Lin, S. Hu, J. Yang, and Y. Xie, Metallic few-layered VS2 ultrathin nanosheets: High two-dimensional conductivity for in-plane supercapacitors, J. Am. Chem. Soc. 133, 17832 (2011).
- [4] K. F. Mak, C. Lee, J. Hone, J. Shan, and T. F. Heinz, Atomically Thin MoS<sub>2</sub>: A New Direct-Gap Semiconductor, Phys. Rev. Lett. 105, 136805 (2010).
- [5] A. Splendiani, L. Sun, Y. Zhang, T. Li, J. Kim, C.-Y. Chim, G. Galli, and F. Wang, Emerging photoluminescence in monolayer MoS<sub>2</sub>, Nano Lett. 10, 1271 (2010).
- [6] K. Watanabe, T. Taniguchi, and H. Kanda, Direct-bandgap properties and evidence for ultraviolet lasing of hexagonal boron nitride single crystal, Nat. Mater. 3, 404 (2004).
- [7] I. Guillamon, H. Suderow, S. Vieira, L. Cario, P. Diener, and P. Rodiere, Superconducting Density of States and Vortex Cores of 2H-TaS<sub>2</sub>, Phys. Rev. Lett. 101, 166407 (2008).
- [8] E. Navarro-Moratalla, J. O. Island, S. Mañas-Valero, E. Pinilla-Cienfuegos, A. Castellanos-Gomez, J. Quereda, G. Rubio-Bollinger, L. Chirolli, J. A. Silva-Guillén, N. Agraït, G. A. Steele, F. Guinea, H. S. J. v. d. Zant, and E. Coronado, Enhanced superconductivity in atomically thin TaS<sub>2</sub>, Nat. Commun. 7, 11043 (2016).
- [9] M. M. Ugeda, A. J. Bradley, Y. Zhang, S. Onishi, Y. Chen, W. Ruan, C. Ojeda-Aristizabal, H. Ryu, M. T. Edmonds, H.-Z. Tsai, A. Riss, S.-K. Mo, D. Lee, A. Zettl, Z. Hussain, Z.-X. Shen, and M. F. Crommie, Characterization of collective ground states in single-layer NbSe<sub>2</sub>, Nat. Phys. 12, 92 (2016).
- [10] G. Liu, S. Rumyantsev, M. A. Bloodgood, T. T. Salguero, M. Shur, and A. A. Balandin, Low-frequency electronic noise in quasi-1d TaSe<sub>3</sub> van der Waals nanowires, Nano Lett. 17, 377 (2017).
- [11] X. Xi, L. Zhao, Z. Wang, H. Berger, L. Forró, J. Shan, and K. F. Mak, Strongly enhanced charge-density-wave order in monolayer NbSe<sub>2</sub>, Nat. Nanotechnol. 10, 765 (2015).
- [12] W. Choi, N. Choudhary, G. H. Han, J. Park, D. Akinwande, and Y. H. Lee, Recent development of two-dimensional transition metal dichalcogenides and their applications, Mater. Today (Oxford, UK) 20, 116 (2017).
- [13] D. V. Rybkovskiy, A. V. Osadchy, and E. D. Obraztsova, Transition from parabolic to ring-shaped valence band maximum

- in few-layer GaS, GaSe, and InSe, Phys. Rev. B **90**, 235302 (2014).
- [14] H. Cai, E. Soignard, C. Ataca, B. Chen, C. Ko, T. Aoki, A. Pant, X. Meng, S. Yang, J. Grossman, F. D. Ogletree, and S. Tongay, Band engineering by controlling vdW epitaxy growth mode in 2D gallium chalcogenides, Adv. Mater. 28, 7375 (2016).
- [15] J. Robertson, Electronic structure of GaSe, GaS, InSe and GaTe, J. Phys. C: Solid State Phys. 12, 4777 (1979).
- [16] S. Lei, L. Ge, Z. Liu, S. Najmaei, G. Shi, G. You, J. Lou, R. Vajtai, and P. M. Ajayan, Synthesis and photoresponse of large GaSe atomic layers, Nano Lett. 13, 2777 (2013).
- [17] Z. Ben Aziza, D. Pierucci, H. Henck, M. G. Silly, C. David, M. Yoon, F. Sirotti, K. Xiao, M. Eddrief, J.-C. Girard, and A. Ouerghi, Tunable quasiparticle band gap in few-layer GaSe/graphene van der Waals heterostructures, Phys. Rev. B 96, 035407 (2017).
- [18] P. Hu, Z. Wen, L. Wang, P. Tan, and K. Xiao, Synthesis of few-layer GaSe nanosheets for high performance photodetectors, ACS Nano 6, 5988 (2012).
- [19] Y. Zhou, Y. Nie, Y. Liu, K. Yan, J. Hong, C. Jin, Y. Zhou, J. Yin, Z. Liu, and H. Peng, Epitaxy and photoresponse of two-dimensional GaSe crystals on flexible transparent mica sheets, ACS Nano 8, 1485 (2014).
- [20] D. J. Late, B. Liu, J. Luo, A. Yan, H. S. S. R. Matte, M. Grayson, C. N. R. Rao, and V. P. Dravid, GaS and GaSe ultrathin layer transistors, Adv. Mater. 24, 3549 (2012).
- [21] H. Serizawa, Y. Sasaki, and Y. Nishina, Polytypes and excitons in  $GaSe_{1-x}S_x$  mixed crystals, J. Phys. Soc. Jpn. **48**, 490 (1980).
- [22] C. S. Jung, F. Shojaei, K. Park, J. Y. Oh, H. S. Im, D. M. Jang, J. Park, and H. S. Kang, Red-to-ultraviolet emission tuning of two-dimensional gallium sulfide/selenide, ACS Nano 9, 9585 (2015).
- [23] H. Chen, Y. Li, L. Huang, and J. Li, Intrinsic defects in gallium sulfide monolayer: A first-principles study, RSC Adv. 5, 50883
- [24] O. D. Pozo-Zamudio, S. Schwarz, M. Sich, I. A. Akimov, M. Bayer, R. C. Schofield, E. A. Chekhovich, B. J. Robinson, N. D. Kay, O. V. Kolosov, A. I. Dmitriev, G. V. Lashkarev, D. N. Borisenko, N. N. Kolesnikov, and A. I. Tartakovskii, Photoluminescence of two-dimensional GaTe and GaSe films, 2D Mater. 2, 035010 (2015).
- [25] W. Kim, C. Li, F. A. Chaves, D. Jiménez, R. D. Rodriguez, J. Susoma, M. A. Fenner, H. Lipsanen, and J. Riikonen, Tunable graphene-GaSe dual heterojunction device, Adv. Mater. 28, 1845 (2016).
- [26] Z. Ben Aziza, H. Henck, D. Pierucci, M. G. Silly, E. Lhuillier, G. Patriarche, F. Sirotti, M. Eddrief, and A. Ouerghi, van der

- Waals epitaxy of GaSe/graphene heterostructure: Electronic and interfacial properties, ACS Nano 10, 9679 (2016).
- [27] X. Li, L. Basile, B. Huang, C. Ma, J. Lee, I. V. Vlassiouk, A. A. Puretzky, M.-W. Lin, M. Yoon, M. Chi, J. C. Idrobo, C. M. Rouleau, B. G. Sumpter, D. B. Geohegan, and K. Xiao, van der Waals epitaxial growth of two-dimensional single-crystalline GaSe domains on graphene, ACS Nano 9, 8078 (2015).
- [28] Y. Ni, H. Wu, C. Huang, M. Mao, Z. Wang, and X. Cheng, Growth and quality of gallium selenide (GaSe) crystals, J. Cryst. Growth 381, 10 (2013).
- [29] S. Hüfner and T. W. Huber, Photoelectron Spectroscopy: Principles and Applications (Springer, Berlin, Heidelberg, 2003).
- [30] C. R. Whitehouse and A. A. Balchin, Structural studies of compounds in the series  $GaS_x$   $Se_{1-x}$   $(0 \le x \le 1)$  grown by iodine vapour transport, J. Mater. Sci. **13**, 2394 (1978).
- [31] J. C. J. M. Terhell, V. A. M. Brabers, and G. E. van Egmond, Polytype phase transition in the series  $GaSe_{1-x} S_x$ , J. Solid State Chem. **41**, 97 (1982).
- [32] G. Arancia, M. Grandolfo, C. Manfredotti, and A. Rizzo, Electron diffraction study of melt- and vapour-grown  $GaSe_{1-x}S_x$  single crystals, Phys. Status Solidi A **33**, 563 (1976).
- [33] D. Olguín, A. Rubio-Ponce, and A. Cantarero, Ab initio electronic band structure study of III-VI layered semiconductors, Eur. Phys. J. B 86, 350 (2013).
- [34] L. Plucinski, R. L. Johnson, B. J. Kowalski, K. Kopalko, B. A. Orlowski, Z. D. Kovalyuk, and G. V. Lashkarev, Electronic band structure of GaSe(0001): Angle-resolved photoemission and *ab initio* theory, Phys. Rev. B 68, 125304 (2003).
- [35] E. L. Shirley, L. J. Terminello, A. Santoni, and F. J. Himpsel, Brillouin-zone-selection effects in graphite photoelectron angular distributions, Phys. Rev. B **51**, 13614 (1995).
- [36] M. Mucha-Kruczyński, O. Tsyplyatyev, A. Grishin, E. McCann, V. I. Fal'ko, A. Bostwick, and E. Rotenberg, Characterization of graphene through anisotropy of constant-energy maps in angle-resolved photoemission, Phys. Rev. B 77, 195403 (2008).

- [37] M. O. D. Camara, A. Mauger, and I. Devos, Electronic structure of the layer compounds GaSe and InSe in a tight-binding approach, Phys. Rev. B 65, 125206 (2002).
- [38] S. Nagel, A. Baldereschi, and K. Maschke, Tight-binding study of the electronic states in GaSe polytypes, J. Phys. C: Solid State Phys. 12, 1625 (1979).
- [39] D. V. Rybkovskiy, N. R. Arutyunyan, A. S. Orekhov, I. A. Gromchenko, I. V. Vorobiev, A. V. Osadchy, E. Y. Salaev, T. K. Baykara, K. R. Allakhverdiev, and E. D. Obraztsova, Size-induced effects in gallium selenide electronic structure: The influence of interlayer interactions, Phys. Rev. B 84, 085314 (2011).
- [40] Z. Ben Aziza, V. Zolyomi, H. Henck, D. Pierucci, M. G. Silly, J. Avila, S. J. Magorrian, J. Chaste, C. Chen, M. Yoon, K. Xiao, F. Sirotti, M. C. Asensio, E. Lhuillier, M. Eddrief, V. I. Fal'ko, and A. Ouerghi, Valence band inversion and spin-orbit effects in the electronic structure of monolayer GaSe, Phys. Rev. B 98, 115405 (2018).
- [41] M.-W. Chen, H. Kim, D. Ovchinnikov, A. Kuc, T. Heine, O. Renault, and A. Kis, Large-grain MBE-grown GaSe on GaAs with a Mexican hat-like valence band dispersion, npj 2D Mater. Appl. 2, 1 (2018).
- [42] K. Rossnagel, E. Rotenberg, H. Koh, N. V. Smith, and L. Kipp, Fermi surface, charge-density-wave gap, and kinks in 2H-TaSe<sub>2</sub>, Phys. Rev. B **72**, 121103(R) (2005).
- [43] T. Eknapakul, P. D. C. King, M. Asakawa, P. Buaphet, R.-H. He, S.-K. Mo, H. Takagi, K. M. Shen, F. Baumberger, T. Sasagawa, S. Jungthawan, and W. Meevasana, Electronic structure of a quasi-freestanding MoS<sub>2</sub> monolayer, Nano Lett. 14, 1312 (2014).
- [44] T. Ohta, A. Bostwick, T. Seyller, K. Horn, and E. Rotenberg, Controlling the electronic structure of bilayer graphene, Science 313, 951 (2006).
- [45] T. Ohta, A. Bostwick, J. L. McChesney, T. Seyller, K. Horn, and E. Rotenberg, Interlayer Interaction and Electronic Screening in Multilayer Graphene Investigated with Angle-Resolved Photoemission Spectroscopy, Phys. Rev. Lett. 98, 206802 (2007).